Materials and Design 169 (2019) 107654

Contents lists available at ScienceDirect

Materials and Design

journal homepage: www.elsevier.com/locate/matdes

Toughening epoxy syntactic foams with milled carbon fibres: Mechanical properties and toughening mechanisms

Sammy He[a,*], Declan Carolan[a,b], Alexander Fergusson[a,b], Ambrose C. Taylor[a]

[a]Department of Mechanical Engineering, Imperial College London, South Kensington Campus, London SW7 2AZ, UK
[b]FAC Technology, 53 Lydden Grove, Wandsworth, London SW18 4LW, UK

HIGHLIGHTS

- Milled carbon fibres increased the properties of lightweight epoxy/hollow glass microsphere syntactic foams.
- Analytical predictions for fracture energy, tensile modulus and strength show excellent agreement to experimental data.
- An impressive 183% increase in fracture energy and 52% increase in tensile strength was achieved.
- A mechanism describing the transition from low to high tensile strength has been proposed for the first time.

GRAPHICAL ABSTRACT

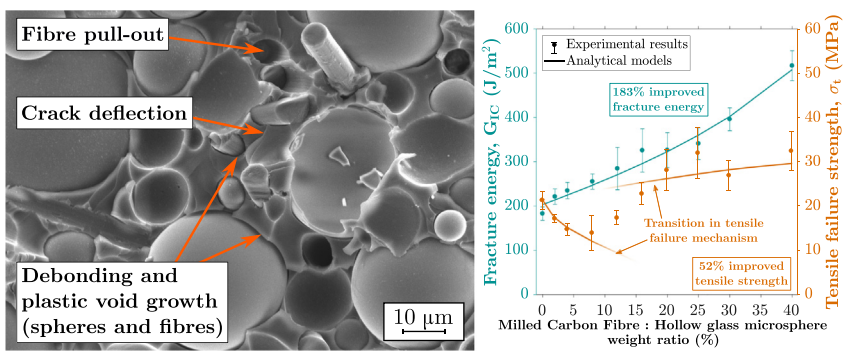

ARTICLE INFO

Article history:
Received 9 January 2019
Received in revised form 8 February 2019
Accepted 9 February 2019
Available online 16 February 2019

Keywords:
Syntactic foam
Hollow glass microspheres
Milled carbon fibre
Tension
Fracture
Toughening mechanisms

ABSTRACT

Syntactic foams comprising hollow glass microspheres (GMS) in an epoxy matrix are critical materials for lightweight structures, being extensively used in marine and aerospace as cores for composite sandwich panels. They are buoyant and crush resistant, but their use is limited by their brittleness. Milled carbon fibres (MCF) were used to increase toughness, by introducing energy absorption mechanisms, to foams comprising ~60 vol% GMS. Weight ratios of up to 40% MCF:GMS were used. The tensile modulus of the foams increased from 3.36 GPa to 5.41 GPa with the addition of 40% weight ratio of MCF. The tensile strength of the syntactic foam decreased with low loadings of MCF, but then recovers when more MCF particles are added, and the mechanisms responsible are explained for the first time. The fracture energy of the syntactic foam increased by 183%, from 182 J/m^2 to 516 J/m^2, due to the addition of 40% weight ratio of MCF. Toughening mechanisms were identified as crack deflection, debonding and subsequent plastic void growth, and fibre pull-out. Thus, the simple and cheap addition of MCF greatly increases the toughness of the syntactic foams, enabling lighter or more damage-resistant structures to be produced.

© 2019 The Authors. Published by Elsevier Ltd. This is an open access article under the CC BY license (http://creativecommons.org/licenses/by/4.0/).

1. Introduction

Syntactic foams have huge potential for lightweight transport applications due to their high specific stiffness. They are composite materials comprising hollow particles in a matrix material. The particles and the matrix may be metal, ceramic, or polymer, or any combination of these. The most important syntactic foam, being

* Corresponding author.
E-mail address: sammy.he12@imperial.ac.uk (S. He).

https://doi.org/10.1016/j.matdes.2019.107654
0264-1275/ © 2019 The Authors. Published by Elsevier Ltd. This is an open access article under the CC BY license (http://creativecommons.org/licenses/by/4.0/).

the lightest and the most commonly used, is hollow glass microspheres (GMS) in an epoxy polymer matrix [1], which is used in the present work. These materials exhibit desirable properties such as low density, high specific strength, high compressive strength, low moisture absorption, and low thermal and electrical conductivity, making them attractive for structural, weight-sensitive applications in the aerospace and marine industries, such as the core in composite sandwich structures [2]. Sandwich structures have seen use in aircraft interior walls, ceilings, floors, and cargo pallets as a means to reduce weight and thus improve fuel efficiency [3]. However, the applications of syntactic foams are limited due to their brittle nature. Defects such as cracks reduce the stiffness and strength of the material, and can propagate with little energy absorption and thus cause catastrophic failure.

One method to improve the fracture toughness is to reduce the GMS volume fraction in the syntactic foam [4], but at a cost of increasing the density since the hollow content provided by GMS is reduced. Another method is the use of nanomodifiers, such as nanoclay [5,6], graphene platelets [7,8], and carbon nanofibres [9,10]. Due to the nanoscale dimensions of these modifiers, they can occupy the spaces between the microspheres, so that densely packed syntactic foams can still be produced. Increases in mechanical and fracture properties have been reported at low volume fractions of nanomodifier. However, these nanomodifiers have a strong tendency to agglomerate at higher volume fractions due to van der Waals interactions between neighbouring nanoparticles [11]. These agglomerations can act as defects in the composite which promote material failure. Indeed, most studies report that the mechanical and fracture properties stagnate or reduce when the volume fraction of nanomodifier is increased, with the exception of the study of nanoclay reinforced syntactic foam by Wouterson et al. [5], where they observed an increase in fracture toughness. They attributed this to the agglomerations being large enough to resist and deflect the crack front, thus absorbing more energy. Modifying syntactic foams with various high aspect ratio microfibres has also been investigated [12-14]. Microfibres can affect the packing factor of the microspheres and thus the density of the syntactic foam, since the sizes of the particles are of a similar order. This is also suggested in simulation results in the literature [15,16]. The studies that modify syntactic foams with microfibres show that the tensile modulus and fracture properties both steadily increase with increasing volume fraction of fibre modifier. However, due to the processing becoming increasingly difficult at high particle loadings, the volume fractions of the modifiers in these studies are low, leading to very modest improvements in toughness (ranging from 25 to 90%). Studies of fibre-reinforced syntactic foams with densely-packed GMS to achieve minimal density are therefore relatively rare. Moreover, the syntactic foams modified with low volume fractions of microfibres showed very little or no increase in tensile failure strength, which is a similar observation to studies which modified bulk polymer matrices (i.e. with no hollow glass microspheres) [17-19]. These studies even report a decrease in tensile failure strength at very low volume fractions of fibres, followed by a recovery at higher volume fractions. A mechanism for this transition in tensile strength behaviour has never been satisfactorily explained.

This study investigates the effect of milled carbon fibre (MCF) particles on the tensile and fracture properties of a syntactic foam. The high modulus and low density of carbon fibre, especially when compared to glass fibres, makes it an ideal candidate for lightweight applications of this type of syntactic foam. Such short fibres are very effective at introducing toughening mechanisms into epoxy composites. In addition, with the expansion of the carbon fibre industry, there is an increasing need for the recycling of carbon fibre from environmental and economic perspectives [20]. MCF is often made from recycled feedstock, and is typically much cheaper than the virgin fibre [21]. Thus, the high-performance, lightweight, sustainable and cheap addition of MCF was selected to enhance the material properties and introduce fibrous toughening mechanisms into the foam. The GMS and MCF particles will be randomly packed, such that the volume fraction of the particles is kept at the maximum for all of the syntactic foam formulations, at around 60%, to minimise density and weight. The tensile modulus, tensile strength, fracture toughness and fracture energy are measured. The toughening mechanisms are then identified using scanning electron microscopy. Various models to predict the tensile modulus, tensile failure strength, and fracture energy are presented and applied. The agreement between the predictions and the measured values is discussed. A mechanism to explain the observed variation in tensile strength is proposed for the first time. This draws on the observed ordering of the MCF in the foam and similarity between electrical percolation and the transition from low to high tensile strength. This work demonstrates that the difficult problem of simultaneously improving the strength and toughness of these materials can be solved by the addition of milled carbon fibre, providing safer and lighter structures enabling more efficient vehicles to be produced.

2. Experimental

2.1. Materials and manufacturing

The matrix for the syntactic foams is an anhydride-cured epoxy polymer. The epoxy resin was a standard diglycidyl ether of bisphenol-A (DGEBA), 'Araldite LY556', with an epoxide equivalent weight (EEW) of 185 g/eq. This was cured using a methyltetrahydrophthalic anhydride, 'Aradur HY917', with an anhydride equivalent weight (AEW) of 166 g/eq. The curing process was accelerated by a heterocyclic amine catalyst, 1-methylimidazole, 'Accelerator DY070'. All epoxy components were supplied by Huntsman, UK. A stoichiometric ratio of 90 parts per hundred resin (phr) of HY917 and 1 phr of DY070 was used.

Bulk plates of the epoxy polymer were cast to determine the matrix properties. The epoxy was prepared by mixing LY556 with HY917 and DY070, followed by degassing in a vacuum oven at 60 °C and −1 atm for 15 min or until no additional air bubbles were formed. This was then poured into release-coated steel vertical moulds of thicknesses 3 mm and 6 mm. The epoxy was cured at 80 °C for 4 h, followed by a post-cure at 140 °C for 8 h as recommended by Huntsman [22].

Borosilicate glass microspheres of type 'S38' from 3M, UK, were used to manufacture the syntactic foams. These microspheres have a mean diameter of 40 μm, a mean wall thickness of 1.28 μm with no porosity, a crush strength of 27.6 MPa (90% survival), a true density of 380 kg/m^3, and no surface treatment [23]. Milled carbon fibres were used as the modifier, supplied as 'Carbiso Mil 100μ' from Easy Composites, UK. The MCF have a mean length of 100 μm and a mean diameter of 7.5 μm, with a true density of 1800 kg/m^3 [24].

The syntactic foams were manufactured so that the hollow glass microspheres are randomly close packed. The volume fraction of GMS in the unmodified syntactic foams should therefore be around 60%, according to the product data sheet [23]. The MCF was added at weight ratios up to 40% MCF:GMS. The required amounts of MCF and GMS were weighed into a beaker and manually mixed by stirring with a spatula until a uniform grey-coloured powder was achieved. This was then passed through a sieve with holes approximately 1.5 mm square several times to remove any large agglomerations of MCF. The mixture was stirred again after each pass through the sieve. This ensured a homogeneous mixture of MCF and GMS. The fibres were added in weight ratios so that the volume fraction of the MCF can be determined after volume fraction analysis of the GMS from optical micrographs, since the volume fraction cannot be calculated directly from weight measurements. This is due to the different geometries the particles, the GMS being spherical and the MCF

being cylindrical. The addition of cylindrical particles will change the packing factor of the spherical particles, which has been shown in computational investigations in the literature [15,16]. From these investigations, it is expected that the total volume fraction of the particles would decrease with increasing MCF content as the MCF are expected to reduce the packing factor of the highly packed GMS.

For the manufacture of the syntactic foams, the epoxy polymer matrix was prepared using the same method described earlier for the bulk plates. The plates of foam were manufactured in a mould and were cured at 80 °C for 4 h, followed by a post-cure at 140 °C for 8 h as recommended by Huntsman [22]. The plates produced were then milled to thicknesses of 3 mm and 8 mm using a TM-2 CNC machine from Haas, UK.

2.2. Mechanical testing

The tensile properties of the bulk epoxy polymer and syntactic foams were determined using uniaxial tensile tests in accordance with the ISO 527-1 [25] test standard. Specimens of type 1BA with a thickness of 3 mm and a gauge length of 25 mm were machined from the plates using a router. At least eight specimens of each syntactic foam formulation were tested at room temperature at a loading rate of 1 mm/min using an Instron 3366 universal testing machine fitted with a 10 kN load cell. The strain was measured using an Instron 2620-601 clip-on extensometer with a 25 mm gauge length. The tensile modulus was calculated over the strain interval of 0.0005–0.0025.

The fracture toughness, K_{IC}, and fracture energy, G_{IC}, were determined using single edge notch bending (SENB) tests in accordance with the ISO 13586 [26] test standard. Specimens of dimensions $80 \times 16 \times 8\,mm^3$ were cut. A V-notch was machined at the mid-length using a horizontal mill to a depth of 5.3 mm. A liquid nitrogen cooled razor blade was then carefully tapped into the V-notch to produce a sharp pre-crack before testing. The specimens were tested at room temperature at a displacement rate of 1 mm/min using an Instron 3366 universal testing machine fitted with a 10 kN load cell. At least ten valid tests were performed for each syntactic foam formulation.

Plane strain compression tests as described by Williams and Ford [27] were conducted on the bulk epoxy polymer to determine the plane strain compressive yield stress, σ_{psc}. Specimens of dimensions $40 \times 40 \times 3\,mm^3$ were first polished to a 3 μm finish using a Saphir 330 polishing machine from ATM, Germany. They were then lubricated with 'High Temperature Grease' from Castrol, UK, and compressed between two 12 mm wide parallel dies, using an Instron 5585H universal testing machine fitted with a 50 kN load cell at a displacement rate of 0.1 mm/min.

2.3. Density

The density of the epoxy matrix was determined using a pyknometer in accordance with the ISO 1183-1 [28] standard. The densities of the syntactic foams were calculated by dividing the mass of the SENB samples by the measured volume.

2.4. Image analysis

A Hitachi S-3400N scanning electron microscope (SEM) was used to observe the fracture surfaces of the SENB samples to identify the toughening mechanisms. The samples were mounted on aluminium stubs using electrically-conducting pressure-sensitive tape and sputter-coated with a 10 nm thick layer of gold to minimise charging. An accelerating voltage of 10 kV was used.

Optical microscopy was used to observe the microstructure of the syntactic foams. Small cross-sections of the samples were cold-mounted using an acrylic resin (VARI-SET 10), and were subsequently ground and polished to a 0.25 μm finish using a Saphir 330 polishing machine from ATM, Germany. The optical micrographs were obtained using an AxioScope.A1 optical microscope from Carl Zeiss, Germany, in reflection mode. Image analysis was performed using an open-source image processing software, ImageJ.

3. Results & discussion

In this section, results from microscopy, tensile, and fracture tests on the MCF modified syntactic foams are described. These are followed by the application of analytical models to explain and predict the measured values of the tensile strength and fracture energy.

3.1. Microstructure

3.1.1. Volume fraction analysis

The microstructure of the syntactic foams was determined using optical and scanning electron micrographs. For the unmodified syntactic foams, the micrographs confirmed that the glass microspheres were densely packed within the epoxy matrix, see Fig. 1. Image analysis was performed to determine the area fraction of the particles. The glass microspheres in the optical micrographs were manually selected in the ImageJ software, and the area fraction of the GMS was calculated. According to the Delesse principle [29-31], a cross-section of a material containing spherical particles will show an area fraction of particles exactly equal to the volume fraction. This is true for a wide range of volume fractions, including those used here, see [30] or [31] for example.

Particle analysis was performed on three different optical micrographs of the unmodified syntactic foam, each with an area of approximately $650 \times 480\,\mu m^2$, corresponding to over 1500 particles. The analysis showed that the microspheres in the unmodified syntactic foam have a volume fraction of 60.7%, as expected in a randomly packed structure. This volume fraction also agrees well with the quoted value of 60% for the packing factor in the 'S38' GMS product data sheet [23].

Milled carbon fibres were used to modify the syntactic foams. Individual, straight carbon fibres can be seen in the SEM images, or as bright spots in the optical micrographs due to their reflective nature, see Fig. 2.

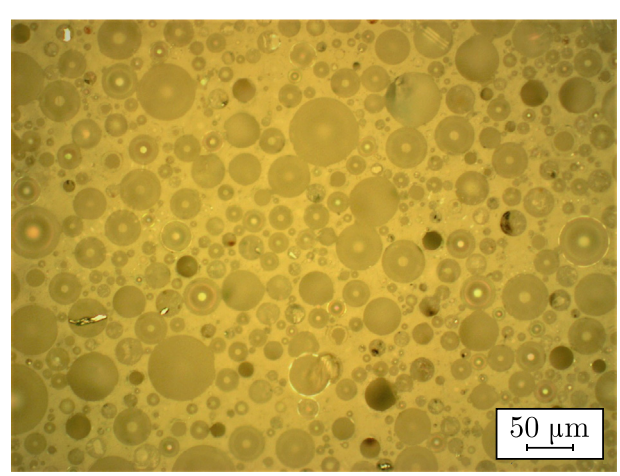

Fig. 1. Optical microscopy image of a cross-section of the unmodified syntactic foam.

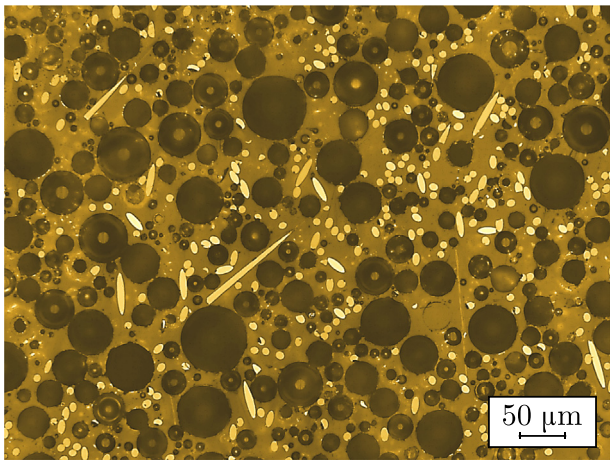

Fig. 2. Optical microscopy image of a cross-section of MCF modified syntactic foam.

Defects such as matrix voids due to air entrapment were present in all syntactic foam formulations, see Fig. 3a. The matrix voids are of a similar size to the microspheres. Rare agglomerations of MCF particles were also present, see Fig. 3b. Agglomerations of up to 500 μm in diameter were observed.

Knowing the volume fractions and densities of the glass microspheres, carbon fibres, and the epoxy polymer, the volume fraction of voids can be calculated, as discussed below in Section 3.1.2. As the volume fraction of voids is constant, i.e. generally independent of the MCF:GMS weight ratio then the voids can be ignored in the volume fraction analysis.

The volume fractions of GMS, MCF and epoxy matrix are related by:

$$V_s + V_f + V_m = 1 \tag{1}$$

where V_s, V_f, and V_m are the volume fractions of the GMS, MCF, and epoxy matrix respectively. The volume fraction of GMS, V_s, is measured directly from the area fraction of the optical micrographs. The volume fraction of the MCF, V_f, can be determined using:

$$V_f = \frac{\rho_s V_s \alpha}{\rho_f (1-\alpha)} \tag{2}$$

where ρ_s is the density of the GMS, ρ_f is the density of the MCF, and α is the MCF:GMS weight ratio used in the manufacturing process. The literature quotes the density of the GMS, ρ_s, as 380 kg/m^3 [23] and the density of the MCF, ρ_f, as 1800 kg/m^3 [24]. The value of α is related to the mass fractions, m, using:

$$\alpha = \frac{m_f}{m_f + m_s} \tag{3}$$

where m_f is the mass fraction of the MCF, and m_s is the mass fraction of the GMS. The remaining term in Eq. (1), the volume fraction of the epoxy matrix, V_m, can then be calculated. The measured volume fraction measurements for GMS are shown in Table 1. The volume fraction of GMS for other remaining MCF:GMS weight ratios are interpolated from these data.

Particle analyses on the modified syntactic foams show that the volume fraction of the GMS reduced by 0.11 from unmodified to 40% weight ratio MCF. The total volume fraction of all particles, $V_s + V_f$, also decreases, which was expected from simulation results in the literature [15,16]. This reduction is due to the combined MCF and GMS being unable to pack as closely as GMS alone.

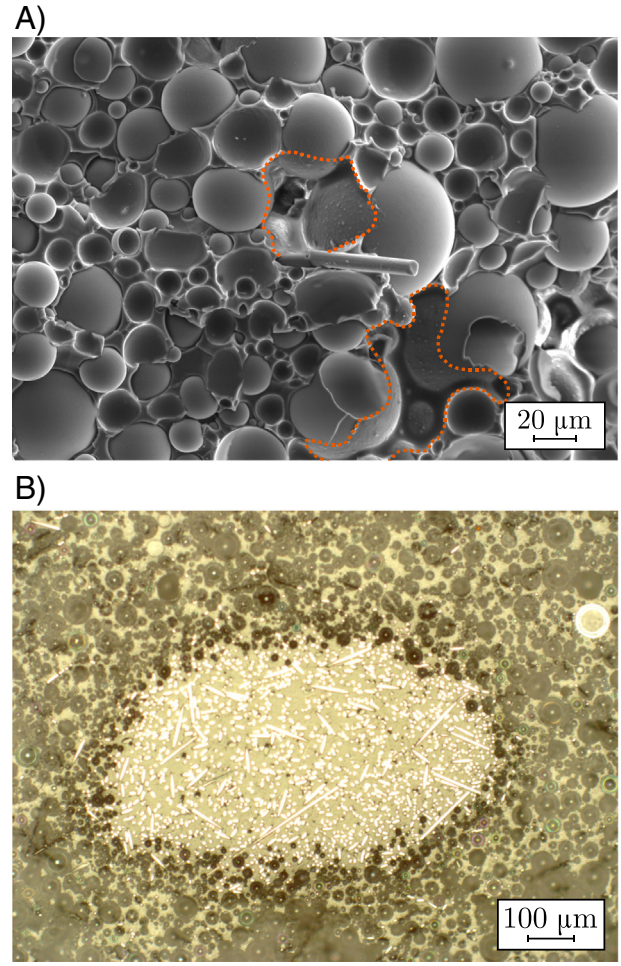

Fig. 3. (a) SEM image of matrix voids (outlined in dashed orange) and (b) optical microscopy image of an agglomeration of MCF particles. (For interpretation of the references to colour in this figure legend, the reader is referred to the web version of this article.)

3.1.2. Density

The densities of the syntactic foams were determined by dividing the mass of the SENB samples by the measured volume. The densities of the syntactic foam formulations are shown in Fig. 4. The density increases from 641 ± 8 kg/m^3 for the unmodified foam, to 797 ± 7 kg/m^3 for the 40% MCF:GMS weight ratio modified syntactic foam. This increase in density was expected due to the high density of the MCF, and due to the volume fraction of GMS decreasing with increasing MCF content. This density increase is small compared to the method of reducing the volume fraction of GMS to increase toughness. Wouterson et al. [4] had found that syntactic foams with 30% volume fraction of GMS showed the greatest toughness, however, this would give a theoretical density of the syntactic foam of 947 kg/m^3 for the materials used in this study. The density of the epoxy matrix, ρ_m, was determined using a pyknometer to be 1190 kg/m^3. The theoretical density of the syntactic foam, ρ_{SF}, can be calculated using:

$$\rho_{SF} = \rho_s V_s + \rho_f V_f + \rho_m V_m \tag{4}$$

The theoretical densities are compared to the measured densities in Fig. 4.

The difference between the measured and the theoretical values is due to the matrix void content in the syntactic foams, as Eq. (4)

Table 1
Effect of MCF:GMS weight ratio on the volume fraction of GMS and MCF.

MCF:GMS weight ratio (%)	MCF:GMS weight ratio, α	GMS, V_s	MCF, V_f	Epoxy, V_m	$V_s + V_f$
0	0	0.607 ± 0.001	0	0.393	0.607
4	0.04	0.584 ± 0.015	0.005	0.405	0.595
8	0.08	0.574 ± 0.003	0.010	0.416	0.584
12	0.12	0.559 ± 0.014	0.016	0.425	0.575
16	0.16	0.547 ± 0.007	0.022	0.432	0.568
25	0.25	0.520 ± 0.012	0.037	0.443	0.557
40	0.40	0.493 ± 0.022	0.069	0.438	0.562

assumes that there are no voids in the foam. Comparison shows that there is matrix void content ranging from 5 to 10%, which is typical for densely packed syntactic foams [32]. This void content is generally independent of the MCF:GMS weight ratio, indicating that the addition of MCF has no detrimental effect on the quality of the syntactic foam.

3.1.3. Fibre orientation

The method of ellipses [33] was applied to the optical microscopy images to determine the orientation of the milled carbon fibres. This method assumes that the fibres can be treated as perfect and rigid cylinders, which is justified in this study as the fibres appear straight on the SEM and optical micrographs. This was expected due to the high modulus of the carbon fibres and low viscosity of the resin. The resin has a low viscosity so the processing of the foams does not cause significant forces on the fibres which would cause bending. A section of a fibre will appear either circular or elliptical, depending on the angle at which it was sectioned. The orientation of a single fibre is dependent on the out-of-plane angle, θ, and the in-plane angle, ϕ. These angles can be used to describe the directional unit vector aligned along the axis of the fibre, **p**:

$$\mathbf{p} = p_1\delta_1 + p_2\delta_2 + p_3\delta_3 \quad (\delta \text{ is the Kronecker delta function}) \tag{5}$$

where p_1, p_2, and p_3 are the Cartesian components of **p**, and are related to θ and ϕ (see Fig. 5a) by:

$$p_1 = \sin\theta\cos\phi \tag{6}$$

$$p_2 = \sin\theta\sin\phi \tag{7}$$

$$p_3 = \cos\theta \tag{8}$$

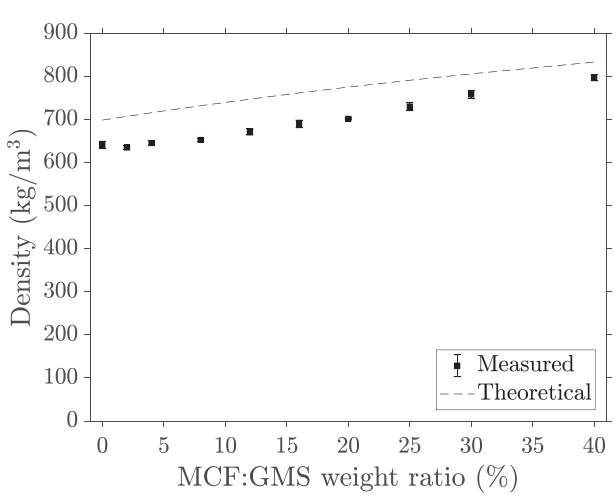

Fig. 4. Density of MCF modified syntactic foams.

The out-of-plane angle, θ, is the inverse cosine of the length of the minor axis, b, over the length of the major axis, a, of the ellipses in the sectioning plane (see Fig. 5b):

$$\theta = \cos^{-1}\left(\frac{b}{a}\right) \tag{9}$$

The in-plane angle, ϕ, is the angle between the in-plane axis (axis 1 in Fig. 5) and the major axis of the ellipse, and can be measured directly from micrographs.

The orientation of a population of fibres can be described by the second-order orientation tensor, A_{ij}, developed by Advani and Tucker [34]:

$$A_{ij} = \langle p_i p_j \rangle = \oint p_i p_j \psi(\mathbf{p})\, \mathrm{d}\mathbf{p} \quad i,j = 1,2,3 \tag{10}$$

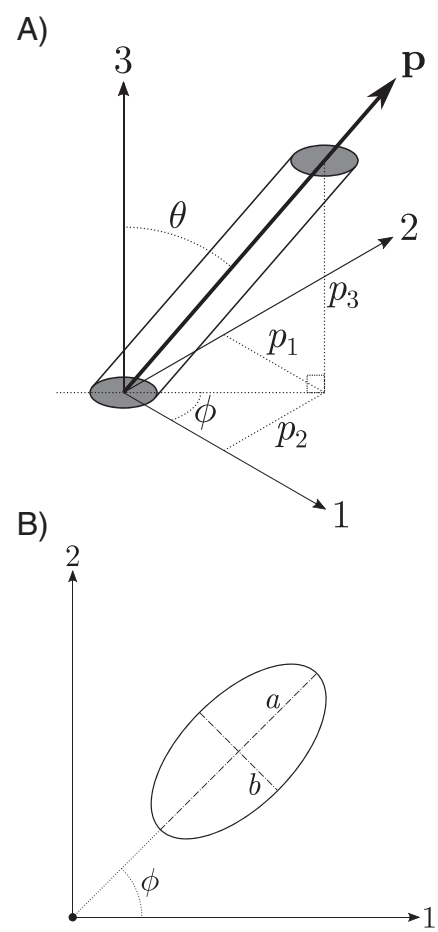

Fig. 5. (a) Co-ordinate system and definitions of θ, ϕ, **p**, and components of **p**. (b) Geometry definitions of an ellipse from a sectioned fibre.

where $\psi(\mathbf{p})$ is the probability distribution function which describes the fibre's orientation state at a point in space. Since every fibre must have some orientation, ψ therefore follows the normalisation condition:

$$\oint \psi(\mathbf{p})\, \mathrm{d}\mathbf{p} = 1 \tag{11}$$

Provided that there are an adequate number in carbon fibres in the cross-sectional image, the second-order tensor can be calculated from the average orientation angles of the ellipses left by the sectioned fibres. A sample size, n, of at least 660 is required for a confidence level of 99% and margin of error of 5%, given an infinite population size. For n number of fibres, the tensor components can be calculated as follows:

$$A_{ij} = \frac{\sum (a_{ij})_n F_n}{\sum F_n} \tag{12}$$

where $a_{ij} = p_i p_j$, such that:

$$\begin{cases} a_{11} = \sin^2\theta \cdot \cos^2\phi \\ a_{22} = \sin^2\theta \cdot \sin^2\phi \\ a_{33} = \cos^2\theta \\ a_{12} = a_{21} = \sin^2\theta \cdot \cos\phi \cdot \sin\phi \\ a_{13} = a_{31} = \sin\theta \cdot \cos\theta \cdot \cos\phi \\ a_{23} = a_{32} = \sin\theta \cdot \cos\theta \cdot \sin\phi \end{cases} \tag{13}$$

The weighting function, F_n, is used to correct the bias caused by the higher probability of fibres with small θ appearing on the cross-section. The weighting function proposed by Bay and Tucker [33] was used:

$$F_n = \begin{cases} \frac{1}{\cos\theta_n} & \text{for} \quad \theta < \theta_c \\ \frac{1}{d} & \text{for} \quad \theta > \theta_c \end{cases} \tag{14}$$

where θ_c is the cut-off angle defined as:

$$\theta_c = \cos^{-1}\left(\frac{d}{l}\right) \tag{15}$$

where d and l are the diameter and length of the carbon fibre respectively.

From Eq. (13), it is shown that the second order tensor is symmetric, and the diagonal components sum to unity due to the normalisation condition (Eq. (11)). The diagonal of the tensor (a_{11}, a_{22}, and a_{33}) represents the probability of the fibre aligning in the corresponding direction, with each diagonal component ranging in value from 0 to 1. Other non-diagonal components describe the tilt of orientation in the corresponding plane, varying from −0.5 to 0.5, with 0 representing no tilt.

One limitation of this method is that there are two possible fibre orientations which can leave the same elliptical footprint in the sectioning plane. Fibres that are at angles ϕ and $\phi + \pi$ are indistinguishable in the cross-section, see Fig. 6.

From the definitions in Eq. (13), tensor components a_{11}, a_{12}, a_{22}, and a_{33} are unaffected by this ambiguity. However, for components a_{13} and a_{23}, only the magnitude can be calculated and the signs are unknown. This ambiguity was overcome by performing fibre orientation analysis on three perpendicular sections to completely characterise the fibre orientation. The co-ordinate system for the plates of syntactic foam is defined in Fig. 7, where plane 1-2 represents the face of the syntactic foam plates and 3 represents the through-thickness direction.

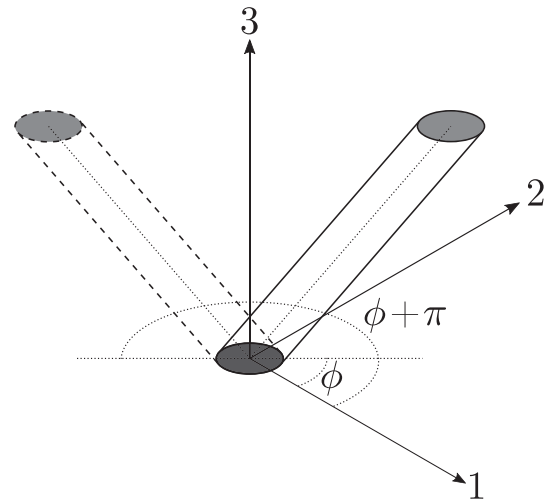

Fig. 6. Ambiguity in fibre orientation from a single cross-section.

Analysis of the micrographs of the perpendicular sections for all volume fractions of MCF, corresponding to over 3000 particles, gives the following tensor:

$$A_{ij} = \begin{bmatrix} 0.427 & -0.044 & 0.011 \\ -0.044 & 0.415 & 0.016 \\ 0.011 & 0.016 & 0.158 \end{bmatrix}$$

This shows that the fibres favour towards a 2D planar orientation in the 1-2 plane, despite the random mixing method of the MCF and GMS particles before the manufacturing process. During mixing, the powder was loosely packed and exhibited some fluidity. Compaction of the mixture to make the densely packed syntactic foam plates may have caused a sedimentation effect, causing fibres initially orientated in the through-thickness direction to settle into an orientation aligned in the 1-2 plane.

3.2. Tension

Tensile tests were conducted on the bulk epoxy polymer and syntactic foam formulations. The measured tensile modulus, E_t, and tensile failure stress, σ_t, of the syntactic foam samples are shown in Fig. 8.

3.2.1. Tensile modulus

The tensile modulus of the bulk epoxy polymer was measured to be 3.27 ± 0.10 GPa, which agrees well with the product data sheet [22]. This increases to 3.36 ± 0.08 GPa with the addition of 60% vol of

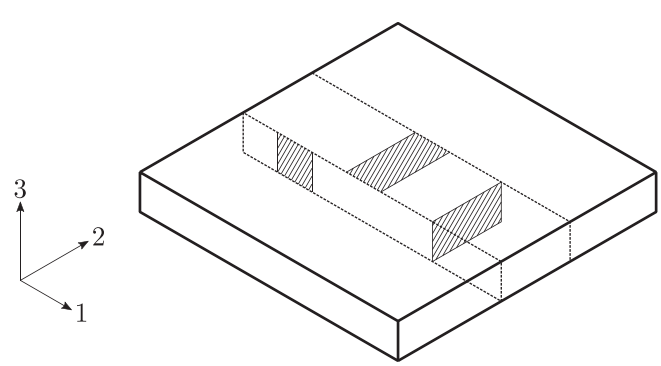

Fig. 7. Perpendicular sectioning and co-ordinate system of the syntactic foam plates.

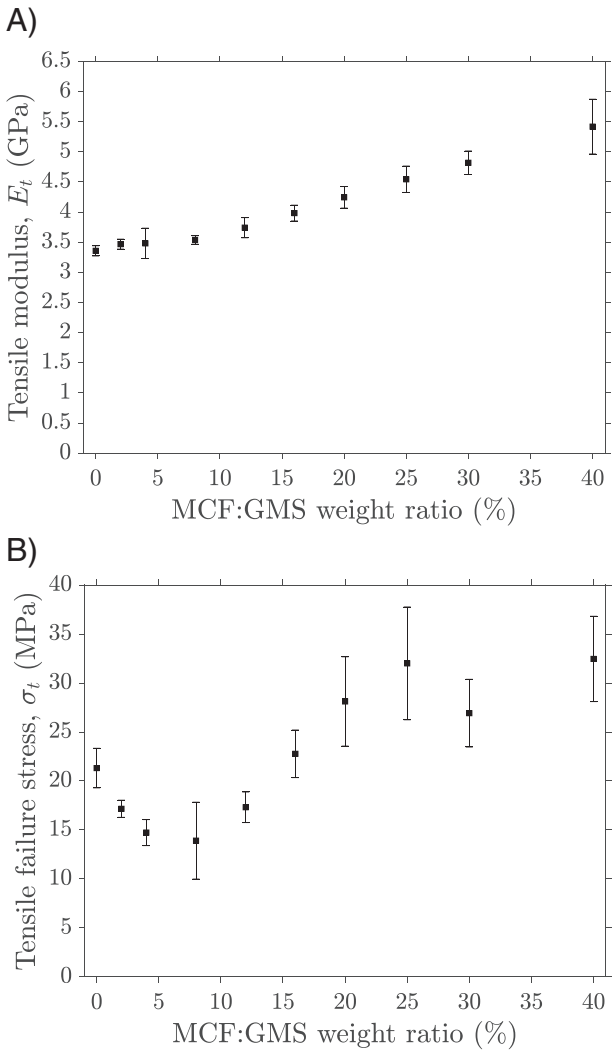

Fig. 8. (a) Tensile modulus and (b) tensile failure stress of MCF modified syntactic foams.

glass microspheres to create the syntactic foam. This was expected due to the higher modulus of the GMS compared to the epoxy. Due to the void content and thin walls, the hollow glass microspheres will have a much lower effective Young's modulus compared to their solid counterparts. The apparent modulus of the microspheres, E_s, can be estimated using an expression developed by Christensen [35], where a micro-mechanics model, the generalised self-consistent method, was used and applied for spherical voids:

$$E_s = E_g\left(\frac{2}{5+3\nu_g}\right)(1-c) \tag{16}$$

where E_g and ν_g are the Young's modulus (63 GPa [36]) and Poisson's ratio (0.2 [36]) of borosilicate glass respectively, and c is the void fraction (i.e. the fraction of the microspheres which is hollow), which is quoted in the manufacturer's datasheet as 0.85 [23]. This gives the apparent modulus of the GMS particles as 3.38 GPa.

The modulus of the syntactic foam can be predicted using the Halpin-Tsai model [37], where the tensile modulus of the composite in a given direction, E_{ii}, is given by:

$$E_{ii} = \frac{1+\zeta_{ii}\eta V_p}{1-\eta V_p}E_m \tag{17}$$

$$\eta = \frac{\frac{E_p}{E_m}-1}{\frac{E_p}{E_m}+\zeta_{ii}} \quad \text{where} \quad i = 1,2 \tag{18}$$

where E_m is the modulus of the matrix, E_p is the modulus of the particle, and V_p is the volume fraction of the particle. The geometry factor, ζ, depends on the particle orientation [37]. For particles aligned in the loading direction, $\zeta_{11} = 2\,(l/d)$, where l and d are the length and diameter of the particle respectively. This will give the parallel composite modulus, E_{11}. For particles aligned in the perpendicular direction, $\zeta_{22} = 2$, giving the perpendicular composite modulus, E_{22}.

The GMS are spherical particles, thus the parallel and perpendicular moduli are equivalent since both ζ values are equal to 2. Substitution of the apparent modulus of the GMS ($E_p = E_s = 3.38$ GPa) into Eq. (18) predicts a modulus of 3.33 GPa for unmodified syntactic foam, which agrees well with the measured value of 3.35 ± 0.08 GPa.

The tensile modulus of the syntactic foam increases with the addition of MCF to 5.42 ± 0.45 GPa at 40% weight ratio of MCF, which is also expected due to the high modulus of the carbon fibre ($E_p = 200$ GPa [24]) compared to that of the unmodified syntactic foam.

The MCF are rod-like (cylindrical) particles where $l = 100\,\mu$m and $d = 7.5\,\mu$m. The modulus in the loading direction therefore depends on the aspect ratio of the fibres, giving $\zeta_{11} = 26.6$ to determine E_{11}. The perpendicular modulus, E_{22}, uses $\zeta_{22} = 2$. The tensile modulus of the composite, E_t, will have contributions from both the parallel and perpendicular moduli components. The magnitude of each of the contributions depends on the orientation of the fibres. Work by van Es [38] described the tensile modulus for composites with 3D randomly orientated fibres as:

$$E_{t,\text{3D random}} = 0.184\,E_{11} + 0.816\,E_{22} \tag{19}$$

In addition, the tensile modulus for composites with 2D planar orientated fibres was described by van Es [38] using laminate theory as:

$$E_{t,\text{2D planar}} = 0.375\,E_{11} + 0.625\,E_{22} \tag{20}$$

The modulus values predicted by application of the Halpin-Tsai model and subsequently, the van Es equations for MCF particles are shown in Fig. 9 for 3D random and 2D planar orientations. The agreement between the predictions for 2D planar orientated fibres and the measured values is excellent, and validates the orientation tensor found by the method of ellipses in Section 3.1.3, which implies 2D planar orientation of MCF in the syntactic foam.

The Halpin-Tsai equations are semi-empirical, and although the model shows good agreement to the experimental results, they have a limited theoretical basis. The Mori-Tanaka model [39] can also be used to predict the tensile modulus of the syntactic foam. The necessary background and equations will be given [39-41]. The Mori-Tanaka model assumes that the matrix, particles, and composite show linear-elastic constitutive behaviour, such that:

$$\boldsymbol{\sigma} = \mathbf{C} : \boldsymbol{\varepsilon} \tag{21}$$

where $\boldsymbol{\sigma}$ and $\boldsymbol{\varepsilon}$ are the stress and strain tensors, and $\mathbf{C}$ is the fourth order linear-elastic stiffness tensor. For an isotropic material, $\mathbf{C}$ is given by:

$$C_{ijkl} = \lambda\delta_{ij}\delta_{kl} + \mu(\delta_{ik}\delta_{jl} + \delta_{il}\delta_{jk}) \tag{22}$$

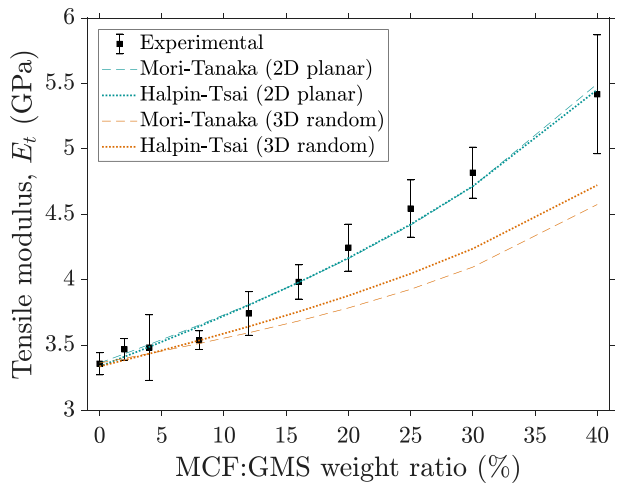

Fig. 9. Halpin-Tsai and Mori-Tanaka modelling of tensile modulus of MCF modified syntactic foams (a false origin has been used on the y-axis to highlight the differences between the models).

where λ and μ are the Lamé constants:

$$\lambda = \frac{E\nu}{(1+\nu)(1-2\nu)} \tag{23}$$

$$\mu = \frac{E}{2(1+\nu)} \tag{24}$$

where E is the Young's modulus, and ν is the Poisson's ratio. The Mori-Tanaka model defines the stiffness tensor of the composite, $\mathbf{C}^c$, in terms of the stiffness tensors of the matrix and the particles:

$$\mathbf{C}^c = \mathbf{C}^m + V_p(\mathbf{C}^p - \mathbf{C}^m)\mathbf{A} \tag{25}$$

where superscripts m and p refer to the matrix and particle respectively, and $\mathbf{A}$ is the strain concentration factor tensor. This concentration factor relates the average strain of the composite, $\bar{\varepsilon}^c$, to the average strain of the particle, $\bar{\varepsilon}^p$, by $\bar{\varepsilon}^p = \mathbf{A}\bar{\varepsilon}^c$.

Now consider a single spheroidal inclusion in an infinite all-matrix medium. There is now a dilute strain concentration tensor, $\mathbf{T}$, which relates the average strain of the matrix, $\bar{\varepsilon}^m$, to the average strain of the single inclusion, $\bar{\varepsilon}^p$, by $\bar{\varepsilon}^p = \mathbf{T}\bar{\varepsilon}^m$. Eshelby [42] developed expressions for $\mathbf{T}$ based on the fourth order tensor called the Eshelby's transformation tensor, $\mathbf{S}$, which depends on the stiffness properties of the matrix material and the aspect ratio of the spheroidal inclusion. The components of $\mathbf{S}$ and can be found in [40] for both spherical and spheroidal inclusions. A large aspect ratio spheroid can be approximated to a fibre. The relation is given by:

$$\mathbf{T} = \left[\mathbf{I} + \mathbf{S}(\mathbf{C}^m)^{-1}(\mathbf{C}^p - \mathbf{C}^m)\right]^{-1} \tag{26}$$

where $\mathbf{I}$ is the fourth order identity tensor. Work by Benveniste [41] developed the Eshelby model further. By applying the homogeneous boundary conditions on the displacements and tractions of the composite, it was observed that the strain concentration factor $\mathbf{A}$ can be expressed in terms of the dilute strain concentration factor $\mathbf{T}$ by:

$$\mathbf{A} = \mathbf{T}[(1-V_p)\,\mathbf{I} + V_p\mathbf{T}]^{-1} \tag{27}$$

The longitudinal modulus, E_{11}, and the transverse modulus, E_{22}, of a unidirectional fibre composite can then be calculated by extracting the components of $\mathbf{C}^c$, using the Mori-Tanaka model [40], and the values found can be substituted into the van Es equations to account for the random or planar orientation of the milled carbon fibres. The predicted values using the Mori-Tanaka model also show excellent agreement to the experimental values when the 2D planar van Es equation was applied, and are nearly identical to the predictions using the Halpin-Tsai model, see Fig. 9. Although both the Halpin-Tsai and Mori-Tanaka models accurately predict the tensile modulus of the MCF modified syntactic foams in this study, the Halpin-Tsai model is known to underestimate the modulus at high volume fractions of filler [43]. Care must therefore be taken if the Halpin-Tsai model is used in preference over the Mori-Tanaka model because of its relative simplicity.

3.2.2. Tensile failure strength

The tensile failure strength of the bulk epoxy polymer was measured to be 88 ± 1 MPa. Due to their highly crosslinked nature, the tensile behaviour of epoxies is very sensitive to defects and can often fracture before reaching yield. The tensile stress-strain curves show that the epoxy polymer failed very slightly before or at the yield point, such that the tensile yield stress can be assumed to be equal to the tensile failure stress, i.e. $\sigma_{yt} = 88$ MPa for the predictions discussed below.

The tensile failure stress decreased to 21 ± 2 MPa when ~60% vol GMS was added to create the syntactic foam. This was expected since it was well known that particles impart a stress concentration on thermoset polymers [44-46]. A decrease in tensile failure strength was observed in syntactic foams modified with up to 8% weight ratio of MCF. The tensile failure strength then recovers when the weight ratio is further increased, see Fig. 8b, to a maximum value of 32 MPa at a weight ratio of 40%.

A number of microstructural features were observed at all particle loadings. The small addition of fibres entrapped air voids as shown in Fig. 3a, which act as points of stress concentration in the syntactic foam, and may promote material failure. A few agglomerations of MCF particles were also evident, see Fig. 3b. Insufficient wetting of the MCF particles by the resin inside these fibrous agglomerations is likely as the resin cannot adequately penetrate the structure of tightly packed fibres. These agglomerations will act as additional stress concentrations, and may promote early failure of the composite.

3.3. Prediction of tensile failure strength

To model the tensile strength of the MCF modified syntactic foams, models for fibre and spherical particle modified composites were used individually and then combined.

3.3.1. Milled carbon fibre modified epoxy

Firstly, the tensile strength of the epoxy polymer modified with MCF only was predicted using the model developed by Baxter [47] for composites with randomly oriented discontinuous fibres. This model utilises the equations for the three failure mechanisms in fibre reinforced composites postulated by Jackson and Cratchley [48]. These mechanisms are longitudinal, shear, and transverse failure, and are dependent on the loading angle, θ, between the stress axis and the fibre axis. Under uniaxial tension, the applied stress, σ_x, is related to the three stress states by:

$$\sigma_x = \frac{\sigma_L}{\cos^2\theta} \quad \text{for small values of} \quad \theta \tag{28}$$

$$\sigma_x = \frac{\tau}{\sin\theta\cos\theta} \quad \text{for intermediate values of} \quad \theta \tag{29}$$

$$\sigma_x = \frac{\sigma_T}{\sin^2\theta} \quad \text{for large values of} \quad \theta \tag{30}$$

where σ_L is the longitudinal stress, τ is the shear stress, and σ_T is the transverse stress of the composite. These equations are then combined with the Tsai-Hill failure criterion [49]:

$$\left(\frac{\sigma_L}{\sigma_{Lu}}\right)^2 + \left(\frac{\sigma_T}{\sigma_{Tu}}\right)^2 - \frac{\sigma_L\sigma_T}{\sigma_{Lu}^2} + \left(\frac{\tau}{\tau_u}\right)^2 = 1 \tag{31}$$

where the additional subscript, u, describes the critical (failure) stress for the respective stress state.

The critical longitudinal stress, σ_{Lu}, can be found by using the shear-lag model developed by Kelly and Tyson [50]:

$$\sigma_{Lu} = \begin{cases} V_f\sigma_f\left(1 - \frac{l_c}{2l}\right) + (1 - V_f)\,\sigma_m & \text{for} \quad l \geq l_c \\ V_f\sigma_f\frac{l}{2l_c} + (1 - V_f)\,\sigma_m & \text{for} \quad l \leq l_c \end{cases} \tag{32}$$

where σ_f is the fracture stress of the carbon fibre, which is taken as 3150 MPa [24], l is the length of the carbon fibre, and σ_m is the tensile strength of the matrix. The critical length of the carbon fibre, l_c, is given by:

$$l_c = \frac{\sigma_f d}{2\tau_u} \tag{33}$$

where d is the fibre diameter, and τ_u is the shear stress at the fibre/matrix interface. Kelly and Tyson identify τ_u as the yield stress under pure shear of the matrix, assuming perfect interfacial adhesion. It is known that the yielding behaviour of glassy polymers is dependent on the hydrostatic pressure [51], and can be assumed to follow the linear Drucker-Prager yield criterion [52-54]:

$$\tau_{vm} = \tau_y - \mu_m P \tag{34}$$

where τ_{vm} is the von Mises shear stress as defined in Eq. (35) [55], τ_y is the shear yield stress of the epoxy polymer, μ_m is the pressure dependent material constant, and P is the mean hydrostatic stress as defined in Eq. (36) [55]. The subscripts 1, 2 and 3 for σ represent the principal stresses.

$$6\tau_{vm}^2 = (\sigma_1 - \sigma_2)^2 + (\sigma_2 - \sigma_3)^2 + (\sigma_3 - \sigma_1)^2 \tag{35}$$

$$P = \frac{1}{3}(\sigma_1 + \sigma_2 + \sigma_3) \tag{36}$$

The value for μ_m can be determined by testing the epoxy polymer in at least two different stress states. In this study, the results from uniaxial tension and plane strain compression were used. In uniaxial tension, the first principal stress is equal to the tensile yield stress $\sigma_1 = \sigma_{yt} = 88$ MPa, and $\sigma_2 = \sigma_3 = 0$, so that Eq. (34) can be written as:

$$\tau_y = \frac{\sigma_{yt}}{\sqrt{3}} + \mu_m\frac{\sigma_{yt}}{3} \tag{37}$$

In plane strain compression, the epoxy polymer is subjected to a biaxial stress state. Assuming that the first principal stress is the stress applied to the dies being forced into the epoxy polymer, then this will be equal to the plane strain compressive yield stress, i.e. $\sigma_1 = \sigma_{psc}$. The stress normal to the axis of the dies is zero, $\sigma_3 = 0$ [27], so it can be shown that the stress along the axis of the dies is $\sigma_2 = \nu_m\sigma_1$, where ν_m is the Poisson's ratio of the epoxy polymer, which is taken as 0.35 [56]. From plane strain compression tests, the plane strain compressive yield stress of the epoxy polymer was measured to be $\sigma_{psc} = 122$ MPa. Eq. (34) in plane strain compression can therefore be written as:

$$\tau_y = \frac{\sigma_{psc}}{\sqrt{3}}\sqrt{\nu_m^2 - \nu_m + 1} - \mu_m\frac{\sigma_{psc}(\nu_m + 1)}{2} \tag{38}$$

Solving Eqs. (37) and (38) simultaneously gives $\mu_m = 0.131$. This small value of μ_m implies that the yield behaviour of the polymer is only weakly dependent on the hydrostatic pressure. Subsequent substitution of this value into either equation gives a shear yield stress of $\tau_y = 54.8$ MPa. As Kelly and Tyson assume perfect interfacial adhesion, using this value for τ_u in the Baxter model overestimates the tensile stress. The exact value of τ_u is not available for this particular study, however, a value of $\tau_u = 51$ MPa was found to be the most suitable to fit the experimental data, which agrees well with the predicted shear yield stress and is more realistic given that no additional surface treatment was performed on the MCF so the interfacial adhesion will be less than perfect.

Substitution of the values into Eq. (33) gives a critical length of $l_c = 231\,\mu$m, which is much larger than the average length of the MCF (100 μm). The effect of this will be discussed below.

The critical transverse stress, σ_{Tu}, has lower and upper limits, and depends on the strength of the interfacial bond between the matrix and fibre. If the interfacial bond is weaker than the matrix, the lower limit of σ_{Tu} can be modelled by considering the fibres as purely defective cylindrical holes, thus reducing the cross-sectional area of the composite. For a square array of fibres, the transverse stress is given by Hull and Clyne [57]:

$$\sigma_{Tu}(\text{min}) = \sigma_m\left[1 - 2\left(\frac{V_f}{\pi}\right)^{\frac{1}{2}}\right] \tag{39}$$

If the interfacial bond is stronger than the matrix, the transverse stress of the composite is equal to the strength of the matrix:

$$\sigma_{Tu}(\text{max}) = \sigma_m \tag{40}$$

Substitution of Eqs. (28)–(30) into Eq. (31), and integrating for all possible angles of θ, the Baxter model for the conditional tensile strength of the composite with MCF only, σ_Q, is:

$$\sigma_Q = \frac{1}{\pi}\int_0^{\pi}\left[\frac{\cos^4\theta}{\sigma_{Lu}^2} + \left(\frac{1}{\tau_u^2} - \frac{1}{\sigma_{Lu}^2}\right)\sin^2\theta\cos^2\theta + \frac{\sin^4\theta}{\sigma_{Tu}^2}\right]^{-\frac{1}{2}}\mathrm{d}\theta \tag{41}$$

The predicted tensile strengths of the MCF modified epoxies using the Baxter model with σ_{Tu}(min) and σ_{Tu}(max) are shown in Fig. 10. A line showing a constant tensile strength of the matrix, σ_m, is also shown. There is little change in the tensile strength due to the length of the MCF being smaller than the critical length, such that little stress transfer occurs between the matrix and the fibre. The minimum transverse stress from Eq. (39) from Hull and Clyne is also shown in Fig. 10, which models the tensile stress of the MCF modified epoxy if the MCF was treated as purely defects.

3.3.2. Glass microsphere and milled carbon fibre modified epoxy

The conditional tensile strengths, σ_Q, calculated above can be used to predict the tensile strength when GMS is added to the MCF modified epoxy to create the syntactic foam. The tensile strength will show a particulate response to the GMS, with the model developed by Nicolais and Narkis [58].

Consider a unit cell filled with n^3 uniformly distributed spherical particles, where at a particular plane perpendicular to the loading direction, the particles occupy a maximum cross-sectional area fraction, A. The Nicolais and Narkis model states that the tensile strength

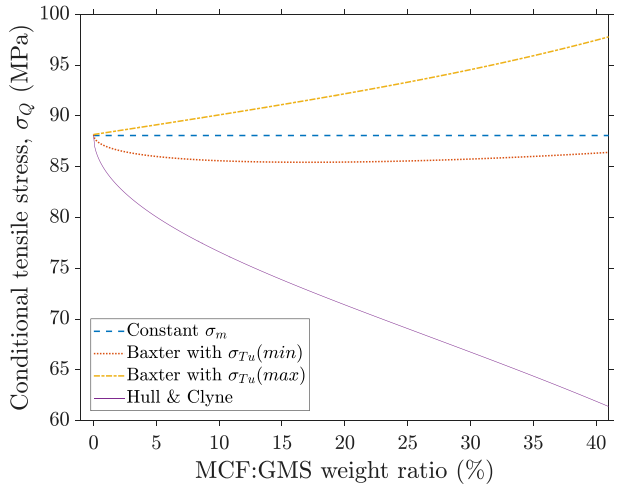

Fig. 10. Predicted tensile strength of MCF modified epoxy using the Baxter and Hull and Clyne models.

of the composite, σ_t, is dependent on the remaining cross-sectional area fraction of the matrix, A_m, such that:

$$\sigma_t = \sigma_Q A_m \tag{42}$$

$$A_m = 1 - A \tag{43}$$

However, the Nicolais-Narkis model assumes no interfacial interaction between the particles and the matrix, essentially treating the particles as voids. Zare [59] developed the original model to take into account the particle-matrix interactions by adding an additional interfacial parameter which includes the interfacial strength, σ_i.

$$\sigma_t = \sigma_Q A_m + \sigma_i A \tag{44}$$

Zare also included an interphase thickness, t, into the area fraction of the particles. An interphase is the small thickness around the particles where the particle-to-matrix adhesion causes this region to have different properties from either the matrix or the particles. For a cubic array of n^3 spherical particles with an interphase thickness, t, which will model the glass microspheres, the maximum cross-sectional area they can occupy on a particular plane is:

$$A = n^2\pi(r+t)^2 \tag{45}$$

where r is the radius of the spheres. The volume of n^3 spherical particles is:

$$V_s = n^3\frac{4}{3}\pi r^3 \tag{46}$$

Making n^2 the subject in Eq. (46) and substituting in Eq. (45) gives:

$$A = \pi\left(\frac{3V_s}{4\pi r^3}\right)^{2/3}(r+t)^2 \tag{47}$$

Substituting Eq. (47) into Eq. (44) gives an expression for the tensile strength of the composite:

$$\sigma_t = \sigma_Q\left[1 - \pi\left(\frac{3V_s}{4\pi r^3}\right)^{2/3}(r+t)^2\left(1 - \frac{\sigma_i}{\sigma_m}\right)\right] \tag{48}$$

The interfacial strength and interphase thickness between the matrix and the microspheres cannot easily be determined. Fitted values of $\sigma_i = 18$ MPa and $t = 1\,\mu$m were chosen to fit the experimental data, and these values agree well with those found in the literature investigating glass fibre/epoxy composites [60-62]. As for the bulk epoxy discussed above, four cases are considered. Eq. (48) is used for when σ_Q is equal to the constant matrix stress σ_m, or the stresses of the MCF modified epoxy from the Baxter model with σ_{Tu}(min) or σ_{Tu}(max). The predictions show good agreement to the experimental results at higher MCF:GMS weight ratios, see Fig. 11. The predictions from using different σ_Q are not significantly different, since there is little change to the stresses predicted by the Baxter model due to the length of the fibres being below the critical length. This shows that the tensile failure strength is more severely affected by the reduction of the volume fraction of the glass microspheres than by the addition of the MCF. The volume fraction of the GMS reduces as the weight ratio increases, effectively increasing the matrix cross-sectional area and thus increasing the tensile strength.

To model the reduction of tensile strength at the lower MCF:GMS weight ratios, the Zare model is added onto the Hull and Clyne equation (Eq. (39)). Hull and Clyne already took into account the reduction in matrix area from the carbon fibres if they were treated as cylindrical holes. Therefore, the area reduction from the GMS particles is added on to the equation, giving:

$$\sigma_t = \sigma_m\left[1 - 2\left(\frac{V_f}{\pi}\right)^{\frac{1}{2}} - \pi\left(\frac{3V_s}{4\pi r^3}\right)^{\frac{2}{3}}(r+t)^2\left(1 - \frac{\sigma_i}{\sigma_m}\right)\right] \tag{49}$$

The predictions from the modified Hull and Clyne model are shown in Fig. 11, and there is excellent agreement between the predictions and the experimental data up to 8% MCF:GMS weight ratio.

3.3.3. Transition in tensile failure strength

It is clear that there is a transition region where the tensile failure strength of the MCF modified syntactic foam goes from where the MCF acts as defects, as in the modified Hull and Clyne model, to where they do not act as defects, as in the constant σ_m or the Baxter model. Several authors [17-19] have also reported decreases in tensile strength at low volume fractions of fibres followed by a recovery at higher volume fractions. Taha and Abdin [17] suggested that there is a critical value of volume fraction where the fibres will as defects

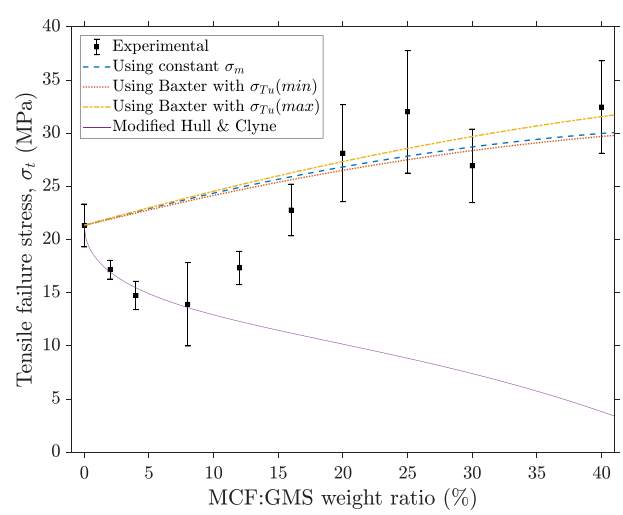

Fig. 11. Predicted tensile failure strength of MCF modified syntactic foams using the Zare model.

in the matrix. How to predict this critical value is currently unclear in the literature.

For this study, the transition region begins to occur at around 10% MCF:GMS weight ratio, which corresponds to a volume fraction of MCF of about 1.3% in the syntactic foam. This is approximately equal to the volume fraction where the electrical percolation threshold occurs for short carbon fibres (SCF), as suggested by [63] and [64]. The electrical percolation threshold is defined as the volume fraction of carbon fibres at which there is a very sharp increase in electrical conductivity in the material. Below this threshold, the fibres act as individual particles, while above this threshold, the fibres form an interconnecting network, allowing flow of electrons from one fibre to another and thus electrical conductivity.

Consider that there is a structural percolation, where instead of a flow of electrons, there is a stress transfer between the carbon fibres. At volume fractions below the structural percolation threshold, the fibres are individual and therefore act as defects, thus reducing the tensile strength. On the other hand, for volume fractions above the structural percolation threshold, since the fibres are interconnected, they are interacting with each other, and not acting as individual defects, hence they do not have a detrimental effect on the tensile strength. The similar value for volume fraction in which both the transition region begins for tensile strength and where electrical percolation threshold occurs, suggests there is a relationship between structural and electrical percolations.

The results from [63] and [64], which investigated the effects of the volume fraction of SCF on the electrical conductivity, are reproduced in Fig. 12. Paligová et al. [63] used SCF with an average diameter of 7 μm and an average length of 270 μm, while Ram et al. [64] used SCF with an average diameter of 6.8 μm, and lengths ranging from 1 mm to 5 mm. This gives electrical data for carbon fibres of aspect ratios (AR) ranging from 38 to 735.

From Fig. 12, the sharp increase in electrical conductivity, and thus the percolation threshold, occurs at increasingly higher volume fractions of SCF as the aspect ratio of the carbon fibre decreases. The electrical conductivity then reaches a steady state at higher volume fractions above percolation threshold. However, the increase in conductivity does not occur instantaneously, but rather within a range of SCF volume fractions. The range broadens as the aspect ratio of the carbon fibres decreases, see Fig. 12. This range to reach steady state conductivity is reminiscent of the broad transition region in the tensile failure strength of MCF modified syntactic foams. The end of the transition region, where the tensile strength of the MCF modified syntactic foam fully recovers to be greater than that of the unmodified foam, occurs at around 20% MCF:GMS weight ratio, see Fig. 11. Above this value the tensile strength shows a steady increase at higher MCF:GMS weight ratios. The end of the transition region corresponds to a volume fraction of MCF of about 2.8% in the syntactic foam. The carbon fibres used in this study have a mean diameter of 7.5 μm, which is similar to those used in [63] and [64], however, the aspect ratio of 13.3 is smaller. Following the trends seen in Fig. 12, it can be expected that for carbon fibres with an aspect ratio of 13.3 that the percolation threshold will occur at a volume fraction somewhere near 1.5%, and the volume fraction to reach steady state conductivity to occur somewhere near 2.5%. These volume fraction values are very similar to those that show a transition in the tensile failure strength of the MCF modified syntactic foams (1.3% to 2.8%). It is concluded that there appears to be a similarity between electrical properties (percolation threshold and steady state conductivity) and tensile failure strength, and this mechanism can explain the observed trend in the strength values.

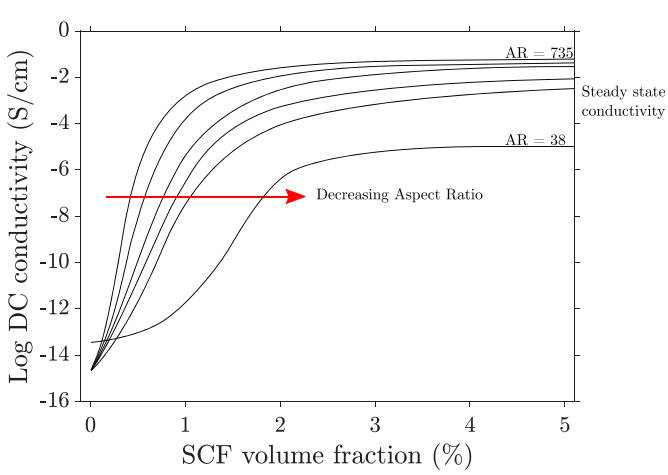

Fig. 12. Log DC conductivity versus SCF volume fraction with different aspect ratios (AR) from 38 to 735.
Source: Reproduced from [63] and [64].

3.4. Fracture

The fracture toughness, K_{IC}, and the fracture energy, G_{IC}, were determined using SENB tests. The recorded curves show linear elastic behaviour, which is expected for these brittle thermoset polymers. The fracture properties were calculated in accordance with the standard, and the results were validated for plane-strain conditions according to the specimen size criteria specified in the test standard [26]. The fracture toughness and energy for the bulk epoxy polymer are $0.61 \pm 0.05\,\text{MPa}\,\text{m}^{1/2}$ and $102 \pm 11\,\text{J/m}^2$ respectively, which shows good agreement to the literature [22]. These values increased to $0.67 \pm 0.08\,\text{MPa}\,\text{m}^{1/2}$ and $183 \pm 15\,\text{J/m}^2$ when ~60 vol% of GMS was added to create the syntactic foam. Both K_{IC} and G_{IC} increase with increasing MCF content, with a fracture toughness of $1.73 \pm 0.07\,\text{MPa}\,\text{m}^{1/2}$ and a fracture energy of $517 \pm 34\,\text{J/m}^2$ being measured for syntactic foam modified with 40% weight ratio of MCF, see Fig. 13. This impressive 182% increase in fracture energy shows good promise for MCF as a toughener for syntactic foams. This study achieved a percentage increase in fracture energy much higher than that in the literature mentioned earlier [12-14], while also maintaining the maximum possible packing factor to minimise density.

3.5. Fractography

Scanning electron microscopy was used to examine the fracture surfaces in the vicinity of the pre-crack tip to determine the toughening mechanisms responsible for the large increases in toughness. The fracture surfaces of the bulk epoxy polymer were found to be smooth and featureless, as is typical for brittle thermoset polymers [65]. When GMS is added to create the syntactic foam, the fracture surfaces show crack deflection, debonding and plastic void growth toughening mechanisms. Crack deflection is evident from the step structures in the epoxy matrix and the characteristic 'tails' behind the rigid particles. When the syntactic foams were modified with MCF, the additional fibre pull-out toughening mechanism can be seen, and is evident from the exposed fibres and cavities left by the fibres on the fracture surface. The fibres also exhibit debonding and plastic void growth.

The different toughening mechanisms are identified on the scanning electron micrograph shown in Fig. 14.

3.6. Prediction of fracture energy

The fracture energy of the modified syntactic foam can be predicted analytically using [66]:

$$G_{IC} = G_{ICU} + \Psi \tag{50}$$

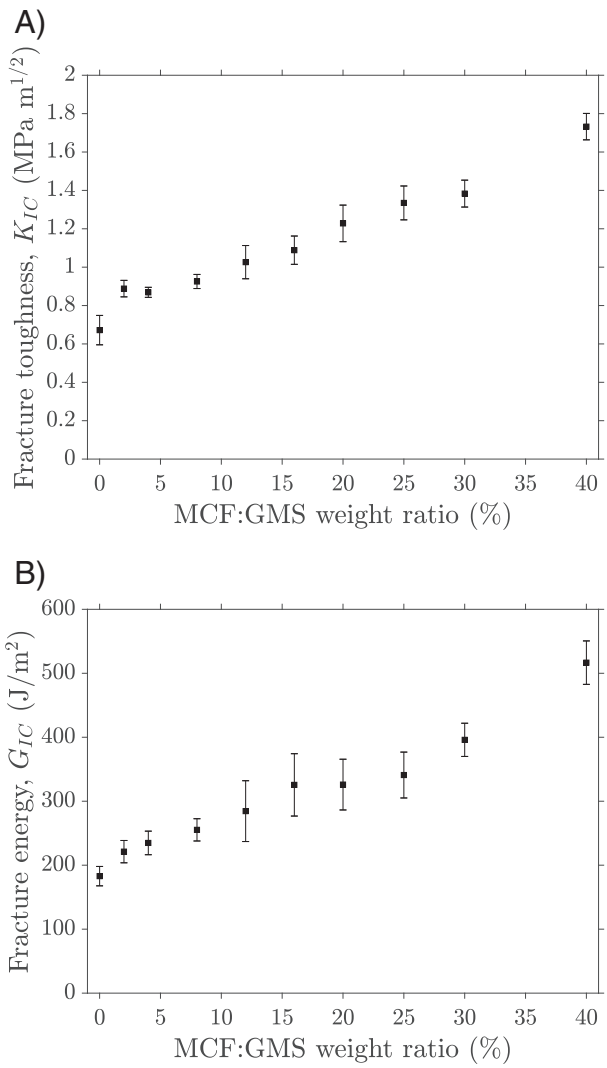

Fig. 13. (a) Fracture toughness and (b) fracture energy of MCF modified syntactic foams.

where G_{ICU} is the fracture energy of the unmodified epoxy and Ψ is the sum of the fracture energy contributions from the toughening mechanisms provided by the GMS and MCF particles. A fracture energy of $G_{ICU} = 102 \pm 11\,\mathrm{J/m^2}$ was measured for the bulk unmodified epoxy, which agrees well with the literature [22]. Each of the toughening mechanisms identified from the fractography will be discussed in turn, and the model used to predict the increase in fracture energy from each mechanism will be introduced. The identified toughening mechanisms were crack deflection from the GMS, debonding and plastic void growth from both the GMS and MCF, and fibre pull-out from the MCF.

3.6.1. Crack deflection

The fracture energy contribution from crack deflection by the GMS, ΔG_{cd}, can be predicted using the Faber and Evans [67] model. The full equations for the crack deflection model can be found in [67], and the toughness prediction graph is reproduced in Fig. 15 for spherical particles of uniform spacing.

This model takes into account the tilt and twist of the crack front when it approaches a rigid particle. The nominally mode I crack is deflected so is subjected to local mixed-mode loading, which increases the strain energy release rate as mode II crack propagation requires more energy than mode I, thus imparting an increase in fracture toughness. This mechanism is applicable provided that the diameter of the particles is larger than the crack tip opening displacement [68,69]. Indeed, work on epoxies modified with nano-sized particles (~20 nm diameter) [70] found that models for crack pinning and deflection mechanisms showed poor agreement with the measured values as the particles were too small to cause these mechanisms.

The crack opening displacement under plane strain conditions, δ_o, can be calculated using [66]:

$$\delta_o = \frac{K_{IC}^2}{E_t \sigma_{yt}} \left(1 - \nu_m^2\right) = \frac{G_{IC}}{\sigma_{yt}} \tag{51}$$

Using $\sigma_{yt} = 88\,\mathrm{MPa}$, and the maximum fracture energy measured in this work of $G_{IC} = 517\,\mathrm{J/m^2}$ for the 40% MCF:GMS weight ratio syntactic foam, a crack opening displacement of 5.9 μm was calculated, which is much smaller than the mean diameter of the glass microspheres of 40 μm. Application of the Faber and Evans model for crack deflection is therefore readily justified in this study.

3.6.2. Debonding

The GMS and the MCF were observed to debond from the epoxy matrix. Hull and Clyne [57] derived an expression to predict the fracture energy contribution from particle debonding, ΔG_{db}:

$$\Delta G_{db} = \int_0^L \frac{V_p}{\pi r^2 L} 2\pi r x_o G_i \quad \mathrm{d}x_o \tag{52}$$

where x_o is the embedded length of the particle in the matrix, L is half the length of the particle, r is the radius of the particle and G_i is the interfacial fracture energy between the particle and the matrix. Integrating leads to the expressions for debonding energy for spheres and fibres respectively:

$$\Delta G_{db,s} = V_s \ln(4) G_{i,s} \tag{53}$$

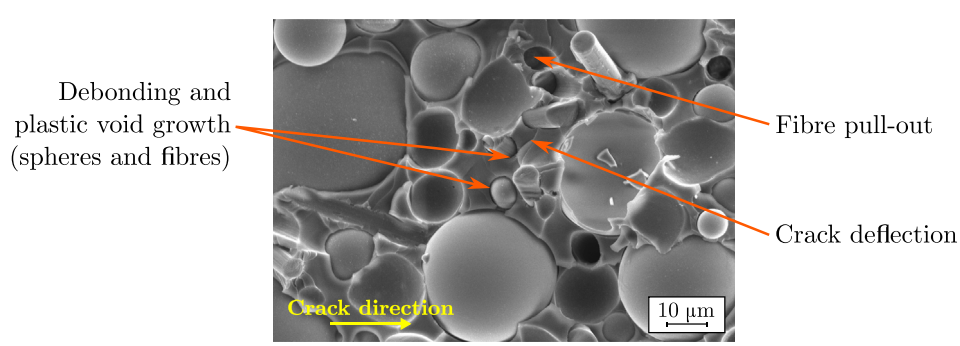

Fig. 14. SEM image of a fracture surface of MCF modified syntactic foam with labelled toughening mechanisms.

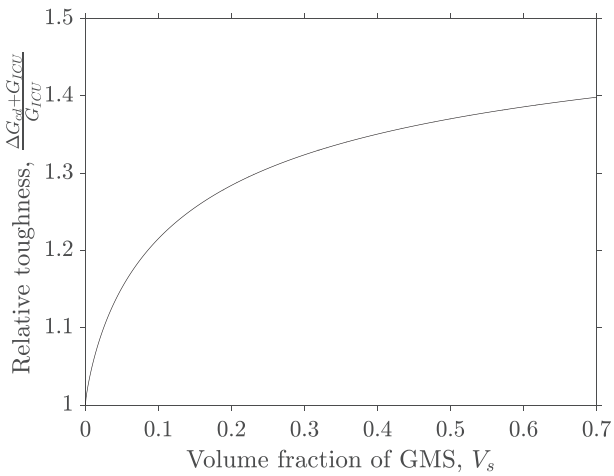

Fig. 15. Relative toughness prediction from crack deflection model for spherical particles of uniform spacing.
Source: Reproduced from [67].

$$\Delta G_{db,f} = \frac{V_f L}{r} G_{i,f} \tag{54}$$

The interfacial fracture energy of carbon fibre in epoxy was determined experimentally by Wang et al. [71] and is taken as $G_{i,f} = 10\,\mathrm{J/m^2}$. For GMS, the interfacial fracture energy, $G_{i,s}$, can be estimated using [72]:

$$G_{i,s} = \frac{3\sigma_{yt}^2 r}{4\pi E_m} \tag{55}$$

Substituting the parameters for the epoxy polymer gives a value of $G_{i,s} = 10\,\mathrm{J/m^2}$, which is similar to values found in literature that investigated glass/epoxy interfaces [73,74].

3.6.3. Fibre pull-out

The MCF undergo pull-out, and the fracture energy contribution from fibre pull-out, ΔG_{po}, was also derived from Hull and Clyne [57]:

$$\Delta G_{po} = \frac{V_f L^2}{3r} \tau_u \tag{56}$$

The value of τ_u is taken as 51 MPa from Section 3.3.1. This equation assumes unidirectional fibre alignment. Since the MCF particles are 2D planar randomly orientated, the fracture energy contribution from particle pull-out will be overestimated. Therefore an fibre orientation efficiency factor, η_o, is used to modify the equation as a correction for this overestimation:

$$\Delta G_{po,2D} = \eta_o \frac{V_f L^2}{3r} \tau_u \tag{57}$$

For 2D planar randomly oriented fibres, it can be shown that the fibre orientation factor is [75]:

$$\eta_o = \frac{1}{\pi} \int_0^{\pi} \cos^4\theta \quad \mathrm{d}\theta \tag{58}$$

where θ is the angle between the fibre axis and the loading axis. This gives a simple numerical value of $\eta_o = 0.375$.

3.6.4. Plastic void growth

When the GMS or the MCF debond, the void created can grow by plastic deformation of the epoxy matrix. The plastic void growth contribution to the fracture energy was calculated using [54]:

$$\Delta G_v = \left(1 - \frac{\mu_m^2}{3}\right)(V_v - V_p)\,\sigma_{yc} r_{yu} K_{vm}^2 \tag{59}$$

where V_v is the volume fraction of the voids created by debonding. The uniaxial compressive yield stress of the matrix, σ_{yc}, is related to the uniaxial tensile yield stress by the following [54]:

$$\sigma_{yc} = \sigma_{yt} \frac{3^{1/2} + \mu_m}{3^{1/2} - \mu_m} \tag{60}$$

The radius of the plastic zone, r_{yu}, can be calculated using the equation proposed by Irwin [76]:

$$r_{yu} = \frac{1}{6\pi}\left(\frac{K_{ICU}^2}{\sigma_{yt}^2}\right) \tag{61}$$

where K_{ICU} is the fracture toughness of the unmodified epoxy. The von Mises stress concentration factor, K_{vm}, varies linearly with the volume fraction of the particles [77]:

$$K_{vm} = 0.59V_p + 1.65 \tag{62}$$

From the SEM micrographs, the voids left by the GMS particles showed an average 8% increase in volume, while voids left by MCF showed an average 32% increase in volume. The fracture energy contribution from plastic void growth can therefore be calculated individually for GMS and MCF by applying the corresponding volume fraction of the particles ($V_p = V_s$ or V_f) and voids in Eqs. (59) and (62).

3.6.5. Predicted fracture energies

The predicted fracture energy contributions from each of the toughening mechanisms are shown in Fig. 16a. The contribution from fibre pull-out becomes the dominant toughening mechanism at higher MCF weight ratios. The contributions from the other toughening mechanisms remain approximately constant, as they depend on the particle volume fraction which does not change significantly (60.7% to 56.2%). The void growth, crack deflection, and debonding mechanisms gives fracture energy contributions of around 55 J/m^2, 39 J/m^2, and 11 J/m^2 respectively. The GMS particles provided the majority of the fracture energy contributions from debonding and void growth due to the much higher volume fractions of GMS compared to MCF. When all of the above models are applied, the fracture energy contributions are summed and added to the fracture energy of the bulk epoxy polymer to give a prediction in the fracture energy of the syntactic foams. Note that the fracture energy of the unmodified syntactic foam is predicted, so does not need to be measured. The predictions in fracture energy shows excellent agreement with the experimental values, see Fig. 16b. Note that these predictions require no fitting to the data, but are derived solely from material properties and observation of the fracture surfaces.

4. Conclusions

Syntactic foams comprising hollow glass microspheres in an epoxy matrix are extensively used in lightweight structures for marine and aerospace, often as the core for sandwich composite panels, but their use in limited by their brittleness. To increase the toughness, foams comprising 60% volume fraction of hollow glass microspheres (GMS) embedded in an epoxy matrix were modified with milled carbon fibre (MCF) with the aim to increase toughness and strength. MCF was selected due to its high specific modulus,

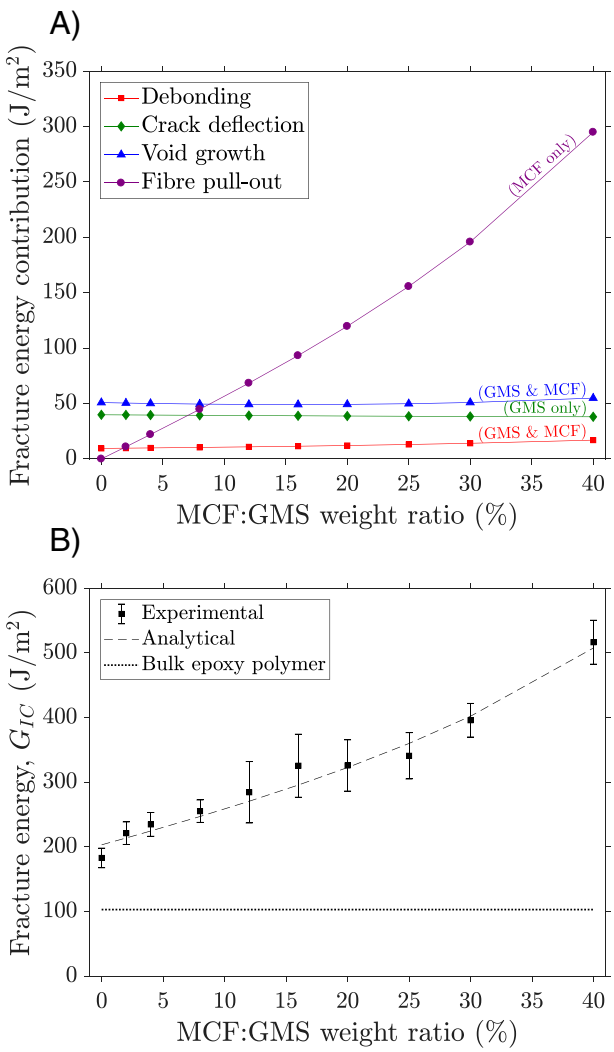

Fig. 16. (a) Fracture energy contributions from identified toughening mechanisms. (b) Analytical and experimental fracture energy of MCF modified syntactic foams.

which is critical in weight-sensitive applications. MCF is also often produced from recycled feedstock, and there is an increasing demand for the recycling of carbon fibre in the expanding industry. The GMS had a mean diameter of 40 μm, and the MCF had a mean diameter of 7.5 μm and a mean length of 100 μm. The tensile and fracture properties of syntactic foams reinforced with milled carbon fibre (MCF) were measured. Milled carbon fibre was added to the glass microspheres (GMS) at different weight ratios.

At 40% weight ratio, the tensile modulus of the syntactic foam increased to 5.41 GPa from 3.36 GPa for the unmodified syntactic foam. The Halpin-Tsai and Mori-Tanaka models for tensile modulus shows very good agreement to the experimental data. The tensile strength of the syntactic foam decreased when low volume fractions of MCF were added, but increased at higher volume fractions. Although this behaviour has been observed previously, an explanation for this transition in tensile strength is lacking. By comparing the tensile strengths with the electrical properties of short carbon fibre reinforced polymers, the mechanisms involved in the transition in tensile strength has been proposed for the first time in the present work. The experimental results showed excellent agreement to analytical models which treat the MCF as defects at low volume fractions, and uses a constant matrix strength at higher volume fractions. The transition occurs at approximately the percolation threshold for MCF. The fracture energy also increased to 517 J/m^2 at 40% MCF:GMS weight ratio from 183 J/m^2 for the unmodified, showing good promise for MCF as a toughener in syntactic foams. Scanning electron microscopy identified the toughening mechanisms as crack deflection, fibre pull-out, and debonding with subsequent plastic void growth. Analytical modelling of these toughening mechanisms showed excellent agreement to the experimental data, and showed that fibre pull-out is the main contributor to fracture toughness at higher loadings of MCF. The significant increases in tensile strength (of over 50%) and fracture energy (of almost 200%) achieved in this study can increase the overall usefulness of syntactic foams in structural applications in the aerospace and marine industries, enabling the design of stronger, lighter, and more fuel-efficient vehicles.

CRediT authorship contribution statement

Sammy He: Methodology, Validation, Formal analysis, Investigation, Data curation, Writing - original draft, Visualization. **Declan Carolan:** Conceptualization, Writing - review & editing, Supervision. **Alexander Fergusson:** Conceptualization, Resources, Supervision, Funding acquisition. **Ambrose C. Taylor:** Conceptualization, Resources, Writing - review & editing, Supervision, Funding acquisition.

Acknowledgments

This work was supported by the Engineering and Physical Sciences Research Council (EPSRC) [grant number EP/N509486/1].

References

[1] H.F. Mark, Encyclopedia of Polymer Science and Technology, Concise, 3rd ed., John Wiley & Sons, Hoboken. 2013.
[2] N. Gupta, S.E. Zeltmann, V.C. Shunmugasamy, D. Pinisetty, Applications of polymer matrix syntactic foams, JOM 66 (2) (2013) 245–254.
[3] A.S. Herrmann, P.C. Zahlen, I. Zuardy, Sandwich structures technology in commercial aviation, in: O. Thomsen, E. Bozhevolnaya, A. Lyckegaard (Eds.), Sandwich Structures 7: Advancing with Sandwich Structures and Materials, Springer, Dordrecht, 2005, pp. 13–26.
[4] E.M. Wouterson, F.Y.C. Boey, X. Hu, S. Wong, Specific properties and fracture toughness of syntactic foam: effect of foam microstructures, Compos. Sci. Technol. 65 (11–12) (2005) 1840–1850.
[5] E.M. Wouterson, F.Y.C. Boey, S.C. Wong, L. Chen, X. Hu, Nano-toughening versus micro-toughening of polymer syntactic foams, Compos. Sci. Technol. 67 (14) (2007) 2924–2933.
[6] A. Asif, V.L. Rao, K.N. Ninan, Nanoclay reinforced thermoplastic toughened epoxy hybrid syntactic foam: surface morphology, mechanical and thermo mechanical properties, Mater. Sci. Eng. A 572 (2010) 6184–6192.
[7] E. Zegeye, A.K. Ghamsari, E. Woldenenbet, Mechanical properties of graphene platelets reinforced syntactic foams, Compos. Part B 60 (2014) 268–273.
[8] R. Ciardiello, L.T. Drzal, G. Belingardi, Effects of carbon black and graphene nano-platelet fillers on the mechanical properties of syntactic foam, Compos. Struct. 178 (2017) 9–19.
[9] L. Zhang, J. Ma, Effect of carbon nanofiber reinforcement on mechanical properties of syntactic foam, Mater. Sci. Eng. A 574 (2013) 191–196.
[10] K.R. Dando, D.R. Salem, The effect of nano-additive reinforcements on thermoplastic microballoon epoxy syntactic foam mechanical properties, J. Compos. Mater. 52 (7) (2018) 971–980.
[11] R. Atif, F. Inam, Reasons and remedies for the agglomeration of multilayered graphene and carbon nanotubes in polymers, Beilstein J. Nanotechnol. 7 (2016) 1174–1196.
[12] E.M. Wouterson, F.Y.C. Boey, X. Hu, S. Wong, Effect of fiber reinforcement on the tensile, fracture and thermal properties of syntactic foam, Polymer 48 (11) (2007) 3183–3191.
[13] J.A.M. Ferreira, C. Capela, J.D. Costa, A study of the mechanical behaviour on fibre reinforced hollow microspheres hybrid composites, Compos. A: Appl. Sci. Manuf. 41 (3) (2010) 345–352.
[14] C. Huang, Z. Huang, Y. Qin, J. Ding, X. Lv, Mechanical and dynamic mechanical properties of epoxy syntactic foams reinforced by short carbon fiber, Polym. Compos. 37 (7) (2016) 1960–1970.
[15] A.V. Kyrylyuk, A. Wouterse, A.P. Philipse, Random packings of rod-sphere mixtures simulated by mechanical contraction, in: M. Nakagawa, S. Luding

(Eds.), Proceedings of the 6th International Conference on Micromechanics of Granular Media, Powders and Grains. 2009, pp. 211–214.
[16] P. Lu, S. Li, J. Zhao, L. Meng, A computational investigation on random packings of sphere-spherocylinder mixtures, Sci. China Phys. Mech. Astron. 53 (12) (2010) 2284–2292.
[17] I. Taha, Y.F. Abdin, Modelling of strength and stiffness of short randomly oriented glass fiber-polypropylene composites, J. Compos. Mater. 45 (17) (2011) 1805–1821.
[18] E. Rojo, M.V. Alonso, M. Oliet, B.D. Saz-Orozco, F. Rodriguez, Effect of fiber loading on the properties of treated cellulose fiber-reinforced phenolic composites, Compos. Part B 68 (2015) 185–192.
[19] S.T. Cholake, G. Moran, B. Joe, Y. Bai, R.K.S. Raman, X.L. Zhao, S. Rizkalla, S. Bandyopadhyay, Improved fracture toughened epoxy matrix system reinforced with recycled milled carbon fibre, Ann. Mater. Sci. Eng. 2 (2) (2015) 1023.
[20] M. Harris, Carbon Fibre: The Wonder Material with a Dirty Secret, The Guardian. March 22 2017, https://www.theguardian.com/sustainable-business/2017/mar/22/carbon-fibre-wonder-material-dirty-secret, Accessed date: 6 February 2019.
[21] F. Barnes, Recycled carbon: addressing the issues of high volume supply, The Composites and Advanced Materials Expo, September 2016, http://www.elgcf.com/assets/documents/CAMX2016-PPT-ELG.PDF, Accessed date: 6 February 2019.
[22] Huntsman Advanced Materials, Technical Data Sheet of Araldite LY 556/Aradur 917/Accelerator DY 070, Huntsman Corporation, Switzerland, 2007.
[23] 3M, Technical Data Sheet of 3M Glass Bubbles S38, 3M, USA, 2010.
[24] Easy Composites, Technical Data Sheet of Carbiso Milled Carbon Fibre, Easy Composites, UK, 2011.
[25] ISO 527-1, Plastics - Determination of Tensile Properties - Part 1: General Principles, International Organization for Standardization, Geneva, 1996.
[26] ISO 13586, Plastics - Determination of Fracture Toughness (G_{IC} and K_{IC}) - Linear Elastic Fracture Mechanics (LEFM) Approach, International Organization for Standardization, Geneva, 2000.
[27] J.G. Williams, H. Ford, Stress-strain relationships for some unreinforced plastics, J. Mech. Eng. Sci. 6 (4) (1964) 405–417.
[28] ISO 1183-1, Plastics - Methods for Determining the Density of Non-cellular Plastics, International Organization for Standardization, Geneva, 2012.
[29] A. Delesse, Procédé mécanique pour déterminer la composition des roches, Ann. Mines 13 (3) (1847) 379–388. (In French).
[30] E.E. Underwood, Quantitative Stereology, Addison-Wesley Pub. Co., Reading, 1970.
[31] P.R. Mouton, Unbiased Stereology: A Concise Guide, The Johns Hopkins University Press, Baltimore, 2011.
[32] N. Gupta, E. Woldesenbet, Characterisation of flexural properties of syntactic foam core sandwich composites and effect of density variation, J. Compos. Mater. 39 (24) (2005) 2197–2212.
[33] R.S. Bay, C.L. Tucker, Stereological measurement and error estimates for three--dimensional fiber orientation, Polym. Eng. Sci. 32 (4) (1992) 240–253.
[34] S.G. Advani, C.L. Tucker, The use of tensors to describe and predict fiber orientation in short fiber composites, J. Rheol. 31 (8) (1987) 751–784.
[35] R.M. Christensen, Effective properties of composite materials containing voids, Proc. R. Soc. Lond. A Math. Phys. Eng. Sci. 440 (1909) (1993) 461–473.
[36] SCHOTT Technical Glass Solutions, Borosilicate Glass Properties, SCHOTT, UK, 2017.
[37] J.C. Halpin, J.L. Kardos, Halpin-Tsai equations: a review, Polym. Eng. Sci. 16 (5) (1976) 344–352.
[38] M.A. van Es, Polymer-Clay Nanocomposites: The Importance of Particle Dimensions, Ph.D. thesis. Faculty of Applied Sciences, Delft University of Technology. 2001.
[39] T. Mori, K. Tanaka, Average stress in matrix and average elastic energy of materials with misfitting inclusions, Acta Metall. 21 (5) (1973) 571–574.
[40] G.P. Tandon, G.J. Weng, The effect of aspect ratio on the elastic properties of unidirectionally aligned composites, Polym. Compos. 5 (4) (1984) 327–333.
[41] Y. Benveniste, A new approach to the application of Mori-Tanaka's theory in composite materials, Mech. Mater. 6 (2) (1987) 147–157.
[42] J.D. Eshelby, The determination of the elastic field of an ellipsoidal inclusion, and related problems, Proc. R. Soc. Lond. A Math. Phys. Eng. Sci. 241 (1226) (1957) 376–396.
[43] M. Loos, Fundamentals of polymer matrix composites containing CNTs, in: M. Loos (Ed.), Carbon Nanotube Reinforced Composites, William Andrew Publishing, Oxford, 2015, pp. 125–170.
[44] R.A. Pearson, A.F. Yee, Influence of particle size and particle size distribution on toughening mechanisms in rubber-modified epoxies, J. Mater. Sci. 26 (14) (1991) 3828–3844.
[45] G. Giannakopoulos, K. Masania, A.C. Taylor, Toughening of epoxy using core-shell particles, J. Mater. Sci. 46 (2) (2011) 327–338.
[46] J. Chen, A.J. Kinloch, S. Sprenger, A.C. Taylor, The mechanical properties and toughening mechanisms of an epoxy polymer modified with polysiloxane-based core-shell particles, Polymer 54 (16) (2013) 4276–4289.
[47] W.J. Baxter, The strength of metal matrix composites reinforced with randomly oriented discontinuous fibers, Metall. Trans. A. 23 (11) (1992) 3045–3053.
[48] P.W. Jackson, D. Cratchley, The effect of fibre orientation on the tensile strength of fibre-reinforced metals, J. Mech. Phys. Solids 14 (1) (1966) 49–64.
[49] V.D. Azzi, S.W. Tsai, Anisotropic strength of composites, Exp. Mech. 5 (9) (1965) 283–288.
[50] A. Kelly, W.R. Tyson, Tensile properties of fibre-reinforced metals: copper/tungsten and copper/molybdenum, J. Mech. Phys. Solids 13 (6) (1965) 329–338.
[51] P.B. Bowden, The Yield Behavior of Glassy Polymers, in: R.N. Haward (Ed.), The Physics of Glassy Polymers, Applied Science Publishers Ltd, London, 1973,
[52] D.C. Drucker, W. Prager, Soil mechanics and plastic analysis or limit design, Q. Appl. Math. 10 (2) (1952) 157–165.
[53] J.N. Sultan, F.J. McGarry, Effect of rubber particle size on deformation mechanisms in glassy epoxy, Fatigue Fract. Eng. Mater. Struct. 13 (1) (1973) 29–34.
[54] Y. Huang, A.J. Kinloch, Modelling of the toughening mechanisms in rubber-modified epoxy polymers - Part II. A quantitative description of the microstructure-fracture property relationships, J. Mater. Sci. 27 (10) (1992) 2763–2769.
[55] A.F. Bower, Governing equations, Applied Mechanics of Solids, CRC Press. 2009, pp. 13–62.
[56] A.J. Kinloch, Adhesion and Adhesives: Science and Technology, 1st ed., Chapman & Hall, London, 1987.
[57] D. Hull, T.W. Clyne, An Introduction to Composite Materials, 2nd ed., Cambridge University Press, Cambridge, 1996.
[58] L. Nicolais, M. Narkis, Stress-strain behaviour of styrene-acrylonitrile/glass bead composite in the glassy region, Polym. Eng. Sci. 11 (3) (1971) 194–199.
[59] Y. Zare, Development of Nicolais-Narkis model for yield strength of polymer nanocomposites reinforced with spherical nanoparticles, Int. J. Adhes. Adhes. 70 (2016) 191–195.
[60] G. Swaminathan, C. Palanisamy, G. Chidambaram, G. Henri, C. Udayagiri, Enhancing the interfacial strength of glass/epoxy composites using ZnO nanowires, Compos. Interfaces 25 (2) (2018) 151–168.
[61] J. Koyanagi, H. Nakatani, S. Ogihara, Comparison of glass-epoxy interface strengths examined by cruciform specimen and single-fiber pull-out tests under combined stress state, Compos. A: Appl. Sci. Manuf. 43 (11) (2012) 1819–1827.
[62] K. Mai, E. Mäder, M. Mühle, Interphase characterisation in composites with new non-destructive methods, Compos. A: Appl. Sci. Manuf. 29 (9–10) (1998) 1111–1119.
[63] M. Paligová, J. Vilčákova, P. Sáha, V. Křesálek, J. Stejskal, O. Quadrat, Electromagnetic shielding of epoxy resin composites containing carbon fibers coated with polyaniline base, Phys. A Stat. Mech. Appl. 335 (3–4) (2004) 421–429.
[64] R. Ram, M. Rahaman, A. Aldalbahi, D. Khastgir, Determination of percolation threshold and electrical conductivity of polyvinylidene fluoride (PVDF)/short carbon fiber (SCF) composites: effect of SCF aspect ratio, Polym. Int. 66 (4) (2017) 573–582.
[65] Y.J. Lim, D. Carolan, A.C. Taylor, Simultaneously tough and conductive rubber-graphene-epoxy nanocomposites, J. Mater. Sci. 51 (18) (2016) 8631–8644.
[66] A.J. Kinloch, R.J. Young, Fracture Behaviour of Polymers, 1st ed. ed., Applied Science Publishers, London, 1983.
[67] K.T. Faber, A.G. Evans, Crack deflection processes - I. Theory, Acta Metall. 31 (4) (1983) 565–576.
[68] A.G. Evans, The strength of brittle materials containing second phase dispersions, Philos. Mag. J. Theor. Exp. Appl. Phys. 26 (6) (1972) 1327–1344.
[69] D.J. Green, P.S. Nicholson, J.D. Embury, Fracture of a brittle particulate composite - Part 2. Theoretical aspects, J. Mater. Sci. 14 (7) (1979) 1657–1661.
[70] B.B. Johnsen, A.J. Kinloch, R.D. Mohammed, A.C. Taylor, S. Sprenger, Toughening mechanisms of nanoparticle-modified epoxy polymers, Polymer 48 (2) (2007) 530–541.
[71] C. Wang, X. Ji, A. Roy, V.V. Silberschmidt, Z. Chen, Shear strength and fracture toughness of carbon fibre/epoxy interface: effect of surface treatment, Mater. Des. 85 (2015) 800–807.
[72] A.N. Gent, Detachment of an elastic matrix from a rigid spherical inclusion, J. Mater. Sci. 15 (11) (1980) 2884–2888.
[73] L.G. Rosenfeld, J.E. Ritter, T.J. Lardner, M.R. Lin, Use of the microindentation technique for determining interfacial fracture energy, J. Appl. Phys. 67 (7) (1990) 3291–3296.
[74] L. Banks-Sills, D. Ashkenazi, A note on fracture criteria for interface fracture, Int. J. Fract. 103 (2) (2000) 177–188.
[75] H. Krenchel, Fibre Reinforcement: Theoretical and Practical Investigations of the Elasticity and Strength of Fibre-reinforced Materials, Akademisk Forlag, Copenhagen, 1964.
[76] G.R. Irwin, Plastic zone near a crack and fracture toughness, Meeting of the 7th Sagamore Ordnance Materials Research Conference, Racquette Lake, New York, USA, 1960, pp. 63–78.
[77] F.J. Guild, R.J. Young, A predictive model for particulate-filled composite materials - Part 1. Hard particles, J. Mater. Sci. 24 (1) (1989) 298–306.